


Electroluminescence and thermal radiation from metallic armchair carbon nanotubes with defectsZu-Quan Zhang * and Jian-Sheng Wang*Department of Physics, National University of Singapore, Singapore 117551, Republic of Singapore*

(Received 9 June 2021; accepted 9 August 2021; published 20 August 2021)

Bias-induced light emission and thermal radiation from conducting channels of metallic armchair carbon nanotubes (CNTs) with defects are studied theoretically within the framework of nonequilibrium Green's function method based on a tight-binding model. Localized states induced by the single vacancy defect and single Stone-Wales defect in the low-energy range enhance electroluminescence significantly while they reduce thermal radiation under zero bias. The influence of the diameters of the CNTs with defects on the radiation is discussed. Radiations from metallic CNTs in thermal equilibrium show black-body-like spectrum. For perfect nanotubes with small diameter, their thermal radiations are nearly independent on the tube diameter due to the confinement of the thermal excitations in the tube's circular direction. Our study is important for optoelectronic applications of CNTs with defects.

DOI: [10.1103/PhysRevB.104.085422](https://doi.org/10.1103/PhysRevB.104.085422)**I. INTRODUCTION**

Single-walled carbon nanotubes (SWCNTs) are quasi-one-dimensional materials possessing extraordinary electrical, mechanical, and optoelectronic properties [1]. They can be metallic, small-gap semiconducting or semiconducting [2,3]. The geometry of a SWCNT can be described by the tube's chiral vector, which is defined by a pair of integers (n, m) [1]. The band structure of a metallic SWCNT shows nearly linear dispersion relation in the low-energy range around the Fermi level. Optical transitions are forbidden in this low-energy range under an external electric field along the tube axis [4]. When the CNTs are stimulated by electrons or photons, significant light emissions can occur due to transitions between pairs of van Hove singularities that are mirror symmetric with respect to the Fermi level.

Electroluminescence (EL) and photoluminescence (PL) from SWCNTs have been studied a lot in semiconducting CNTs experimentally [5–8]. In contrast, observations of EL from metallic SWCNTs are much less frequent [9–11]. Electroluminescence from suspended metallic SWCNTs are explained by Joule heating [9], and the emission spectrum is different from black-body-like emissions discovered in nanotube bundles and multiwalled CNTs [12–14]. The important role of phonons in light emission has been stressed in recent experiments, where a side peak close to the main transition peak due to phonon-assisted emission appears in the radiation spectrum [10,11].

Defects in CNTs are widely studied and they are shown to have significant influences on various properties of CNTs, such as electric and magnetic properties [15–17], transport properties [18–21], field emission [22], mechanical, and optical properties [23–27]. Common atomic-scale defects in CNTs are vacancies, adatoms, and Stone-Wales (SW)

reconstruction [1,28]. Recent experiments showed that defects can be engineered to tune the optic properties of the CNTs [29], such as enhancing the PL and tuning the single photon emission by sp^3 defects [30–32]. In contrast, the influence of defects on the EL from CNTs is challenging and less studied [33–35]. A recent experiment showed that a local defect could be induced by injecting tunneling electrons from a scanning tunneling microscope (STM) tip to a multiwalled CNT and corresponding changes of EL due to the defect were observed [35]. Theoretically, bias-induced light emission from the nanoscale system has received much attention in recent years [36–41], especially in molecular junctions. However, few works have taken into account of the full geometry of the system at the atomic-scale level. Quantitative calculations of EL from metallic SWCNTs and also taking into account of the influence of defects would be helpful to related experiments.

In this work, we consider a two-terminal device to study the EL from the conducting channels of metallic SWCNTs under the influences of the single vacancy (SV) defect and the single SW defect. The metallic carbon nanotubes studied here are restricted to the gapless armchair nanotubes. We consider electron transport in the ballistic regime without electron-phonon interaction. This can be reasonable when the length of the conducting channel is much smaller than the electron mean free path of the metallic SWCNT, which is about several micrometers [42]. By turning off the applied bias in the device, we also study the thermal radiation from perfect and defected CNTs.

II. MODEL AND METHOD

We describe the Hamiltonian of the electrons in the CNT using the nearest-neighbor (NN) tight-binding (TB) model

$$H_0 = - \sum_{\langle ij \rangle} t_{ij} c_i^\dagger c_j, \quad (1)$$

*phyzhaz@nus.edu.sg

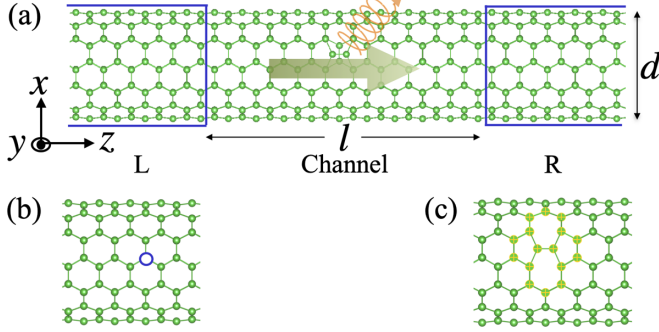


FIG. 1. Illustration of a two-terminal transport device of a SWCNT. (a) The left (L) and right (R) leads are semi-infinite extensions of the pristine carbon nanotube with diameter d , and central region is the conducting channel with a finite length l . The interaction of electrons with the EM field is included only in the central region. The driving current in the central channel induces light emission. (b) A single vacancy defect in the channel, with the missing atom denoted by a blue ring. (c) A Stone-Wales defect in the channel. The structures of nanotubes are drawn using VESTA 3 [43].

where t_{ij} is the hopping parameter, c_i^\dagger (c_j) is the electron creation (annihilation) operator on site i (site j), the angular bracket $\langle ij \rangle$ denotes NN sites. We introduce the coupling of the electrons with the electromagnetic field in free space by using the Peierls substitution, i.e., substituting in Eq. (1) via $t_{ij} \rightarrow t_{ij} e^{i\theta_{ij}}$, with the phase factor $\theta_{ij} = \frac{e}{\hbar} \int_{r_j}^{r_i} \mathbf{A} \cdot d\mathbf{l}$. Here $e = -|e|$ is the electron charge, \hbar is the reduced Planck constant, and \mathbf{A} is the vector potential for describing the free-space electromagnetic field. The coupling of the electrons with the electromagnetic field in the lowest-order approximation can be obtained by expanding θ_{ij} in terms of \mathbf{A} to the linear term, given by

$$H_{\text{int}} = \sum_{\langle ij \rangle} \sum_k \sum_{\mu=x,y,z} M_{ij}^{k\mu} c_i^\dagger c_j A_\mu(\mathbf{r}_k). \quad (2)$$

Here the electron-photon coupling matrix is $M_{ij}^{k\mu} = i \frac{e}{2\hbar} t_{ij} (\mathbf{r}_i - \mathbf{r}_j)_\mu (\delta_{ki} + \delta_{kj})$.

The EL from a SWCNT is considered by a typical two-terminal device under a bias voltage, as shown in Fig. 1(a). The device consists of three parts. The left and right leads are semi-infinite extensions of the pristine CNT. The central part is the conducting channel and it has a finite length. We take into account the interaction of electrons with the EM field only in the central region. Upon applying a bias voltage, an electric current flows through the channel, and photons are excited and emitted due to the inelastic scattering of electrons interacting with the electromagnetic field. The cases that the channel contains a SV defect or a single SW defect are shown in Figs. 1(b) and 1(c), respectively. The SV defect is modeled by using a large onsite energy of 10^6 eV for the vacant atom, and the SW defect is formed by rotating a C–C bond by 90 degrees. The effects of structure relaxations due to the defects are not considered in this paper. Also, we consider the NN hopping parameter $t_{ij} = t$ as a constant.

Radiation from the device is calculated using the nonequilibrium Green's function (NEGF) method based on our previous work [44–47]. The important quantity is the local

current-current correlation function. Its lesser component can be expressed in the random phase approximation as

$$\begin{aligned} \Pi_{\mu\nu}^<(\mathbf{r}_i, \mathbf{r}_j; \omega) &= -i\hbar \int_{-\infty}^{\infty} \frac{dE}{2\pi\hbar} \text{Tr}[M^{i\mu} g^<(E) M^{j\nu} g^>(E - \hbar\omega)], \quad (3) \end{aligned}$$

where $\text{Tr}[\dots]$ stands for trace over the electron degrees of freedom. The electron's lesser (greater) Green's function (GF) without coupling to the EM field is given by $g^{<(>) } = g^r \Sigma_{\text{leads}}^{<(>) } g^a$, with the retarded GF $g^r(E) = [(E + i\eta)I - H_0 - \Sigma_{\text{leads}}^r]^{-1}$, and advanced GF $g^a = (g^r)^\dagger$. I is the identity matrix and η is the GF infinitely small quantity. Σ_{leads}^r is the total self-energy of the two semi-infinite leads, which are calculated by using the recursive GF method [48]. Each lead is in equilibrium and follows the fluctuation-dissipation theorem, obeying the relation $\Sigma_p^< = -f_p(\Sigma_p^r - \Sigma_p^a)$, with $p = L, R$ being the lead indices. $f_p(E, \mu_p) = 1/[\exp(\frac{E - \mu_p}{k_B T_p}) + 1]$ is the Fermi distribution function, k_B is the Boltzmann constant, μ_p and T_p are the temperature and chemical potential of the lead, respectively.

Using the monopole approximation and ignoring the screening effect on current fluctuations, the radiation power and rate of the photon counts (number of photons emitted per unit time) in the far field are given by [46]

$$P = - \int_0^\infty \frac{d\omega}{2\pi} \frac{\hbar\omega^2}{3\pi\epsilon_0 c^3} \sum_\mu \text{Im}[\Pi_{\mu\mu}^{\text{tot},<}(\omega)], \quad (4)$$

$$\frac{dN}{dt} = - \int_0^\infty \frac{d\omega}{2\pi} \frac{\omega}{3\pi\epsilon_0 c^3} \sum_\mu \text{Im}[\Pi_{\mu\mu}^{\text{tot},<}(\omega)], \quad (5)$$

where ϵ_0 is the vacuum permittivity, c is the speed of light, and $\Pi_{\mu\nu}^{\text{tot},<}(\omega) = \sum_{ij} \Pi_{\mu\nu}^<(\mathbf{r}_i, \mathbf{r}_j; \omega)$ is the total current-current correlation function.

III. NUMERICAL RESULTS AND DISCUSSION

In the numerical calculation, we set the bias voltage between the two leads to be symmetric, with $\mu_L = -\mu_R = eV/2$. The C–C bond length is $a = 1.42 \text{ \AA}$. The NN hopping parameter is $t = 2.7 \text{ eV}$ [49]. We use $\eta = 0.10 \text{ meV}$ for the ballistic transport. In this work, we consider the metallic CNTs to be armchair type and we do not consider spins of electrons. Temperatures for the two leads are both set to be 300 K unless stated otherwise. Restricted by the computational cost, we use the central CNT channel with the length $l = 10\sqrt{3}a$.

First, we consider a typical metallic SWCNT with chiral index (7, 7) for the two-terminal device. We compare the results in each plot of Fig. 2 for the cases that the CNT channel containing a single SW defect (SWD), a single SV defect (SVD), and no defect, respectively. As shown in Fig. 2(a), for a perfect CNT, with the increasing of the bias voltage, the photon counts are very small and little changed in the low bias range until the onset of bias at about 2.4 V, which implies the opening of the M_{11} transition between the two van Hove singularities shown by the density of states (DOS) in Fig. 2(c). Below the onset of bias, thermal radiation is small but dominant for the perfect CNT.

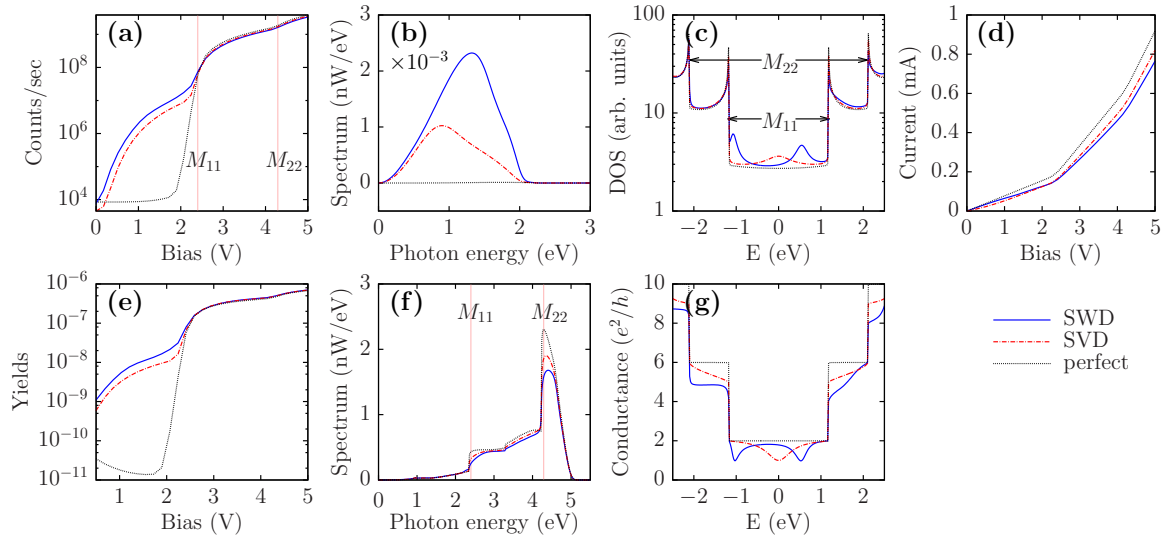


FIG. 2. Results for the two-terminal device of the CNT with chiral index (7, 7). Three curves are shown in each figure, for the CNTs with a single SW defect, a single SV defect, and the perfect one without defect respectively. (a) Photon counts per second and (e) yields from the CNT under a bias voltage. (b) and (f) show the spectrum of the radiation power under the bias voltages 2.0 V and 5.0 V, respectively. (c) The total density of states of the electrons in the channel. (g) The conductance and (d) the I - V curve.

However, when the CNT channel contains a single SW defect or a single SV defect, the photon counts for the two cases increase almost exponentially in the low bias range, while the first is about two times as large as the second. We plot in Figs. 2(b) and 2(f) the spectrum of the radiation power, which is defined as $S(\omega) = -\frac{\omega^2}{6\pi^2\epsilon_0c^3} \sum_{\mu} \text{Im}[\Pi_{\mu\mu}^{\text{tot},<}(\omega)]$ from the integrand of Eq. (4), setting the bias below and above the onset of bias for the M_{11} transition, respectively, with $V = 2.0$ V and $V = 5.0$ V. The spectrum in Fig. 2(b) shows that the average energy of the emitted photons from the CNT with a SW defect is larger than that from the CNT with a SV defect. The radiation spectra for the perfect CNT and the defected CNTs under a large bias show little difference in Fig. 2(f), where the influence of the defects on the radiation is not obvious due to the strong transitions from high-energy bands. To analyze the enhancement of EL in the low-energy range, we plot in Fig. 2(c) the DOS of the CNT channel. There are extra peaks of the DOS in the low-energy range induced by the defects. These localized states account for the EL in the low bias range. For the CNT with a SV defect, the localized state locates near the Fermi level, and for the case with a SW defect, the localized states are away from the Fermi level, close to the edge of the first pair of the van Hove singularities. Thus, the localized states due to a SW defect induce transitions to emit photons with higher energy on average than that with a SV defect. Also, compared with that of the perfect CNT, the electric current in Fig. 2(d) decreases more significantly for the case with a SV defect than that with a SW defect in the low bias range. The localized states due to the defects in the low-energy range reduce the conductance by one quantum unit, as shown in Fig. 2(g). The emission yield, i.e., the number of photons emitted per electron injected into the device channel, is an important quantity to characterize the emission efficiency of the device. Here, the defects can enhance the counts and decrease the electric current, thus they enhance the yields of the EL, as shown in Fig. 2(e). The yields

can reach the order of 10^{-7} in the high bias range, which is consistent with experimental values [50].

In Fig. 3, we discuss the influence of the diameter of the CNT to the EL. Specifically, We consider four different armchair CNTs with the chiral index (n, n) ranging from

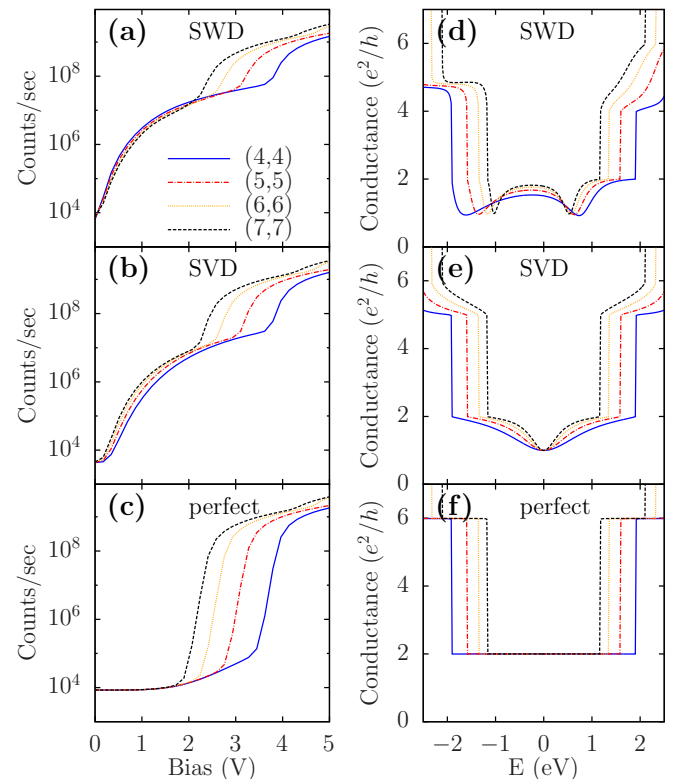


FIG. 3. Photon counts per second (left panel) and conductance (right panel) for the two-terminal device using CNTs with different diameter, with the chiral index (n, n) ranging from $n = 4$ to $n = 7$.

$n = 4$ to $n = 7$. Their diameters are $d = 5.42 \text{ \AA}$, 6.78 \AA , 8.14 \AA , and 9.49 \AA , respectively. There are distinct features for the ELs from the CNTs with different diameters, though the overall trends are similar, as shown in Figs. 3(a) to 3(c). First, plots for the counts from CNTs with different diameters formed some “bubbles” in the high bias range for the CNTs with defects in Figs. 3(a) and 3(b), and the perfect CNTs in Fig. 3(c). This is due to the fact that the transition energy corresponding to the M_{11} gap decreases with the increasing of the tube diameter, which is shown from the conductance plots in Figs. 3(d) to 3(f). Second, the dependence of the counts on the tube diameter is very different for perfect CNTs and defected CNTs under low bias. When the bias is smaller than the onset bias of M_{11} transition, photon counts are inversely proportional to the tube diameter for SW defected CNT, and they are proportional to the tube diameter for SV defected CNT, while they are nearly independent of the tube diameter for the perfect CNT, as shown in Figs. 3(a) to 3(c), respectively. In the low bias range, thermal radiation is dominant over the EL for the perfect CNTs. The energy dispersion relation in the low-energy range accounts for the electron transport in the longitudinal direction along the tube axis and it is of little difference for the CNTs with different diameters, so they show little dependence of thermal radiation on the tube diameter in Fig. 3(c).

We plot in Fig. 4 the thermal radiation from the CNT channel of the two-terminal device by turning off the bias voltage. Figure 4(a) shows that the radiation power of the perfect CNT and the defected CNTs versus the temperature follows the T^4 scaling law as the black-body (BB) radiation. However, the intensity is about two orders of magnitude smaller than the black-body radiation. Figure 4(b) shows the spectrum of the thermal radiation. Both the perfect and defected CNTs show black-body-like radiation, i.e., their spectra fit well with that of the black-body radiation despite the magnitude is smaller. The fitting of the spectrum with the black-body radiation is shown in Fig. 4(c), with the perfect CNT as an example.

Why do the thermal radiations from the quasi-one-dimensional CNTs follow the black-body-like spectrum and they are reduced by the defects? To understand this, we start from the general expression in Eq. (4) to analyze the spectrum of the radiation power. The optical conductivity is related to the retarded component of the current-current correlation function as $\sigma(\omega) = \frac{i}{A\omega} \Pi^r(\omega)$, with $A = \pi dl$ the area of the central CNT channel. Using the fluctuation-dissipation relation in thermal equilibrium $\Pi^<(\omega) = iN_B(\omega)2\text{Im}[\Pi^r(\omega)]$, with $N_B(\omega)$ the Bose distribution function, we can write from Eq. (4) the spectrum of the radiation power in thermal equilibrium as

$$S(\omega) = \frac{A\omega^3}{3\pi^2\epsilon_0c^3} \text{Re}[\sigma^{\text{tot}}(\omega)]N_B(\omega). \quad (6)$$

Here we use the notation $\sigma^{\text{tot}}(\omega) = \sum_{\mu=x,y,z} \sigma_{\mu\mu}(\omega)$. The optical conductivity is calculated by

$$\sigma_{\mu\nu}(\omega) = \frac{1}{A} \int_{-\infty}^{\infty} \frac{dE}{2\pi\omega} \sum_{ij} \text{Tr}[M^{i\mu} g^r(E) M^{j\nu} g^<(E - \hbar\omega) + M^{i\nu} g^<(E) M^{j\mu} g^r(E - \hbar\omega)]. \quad (7)$$

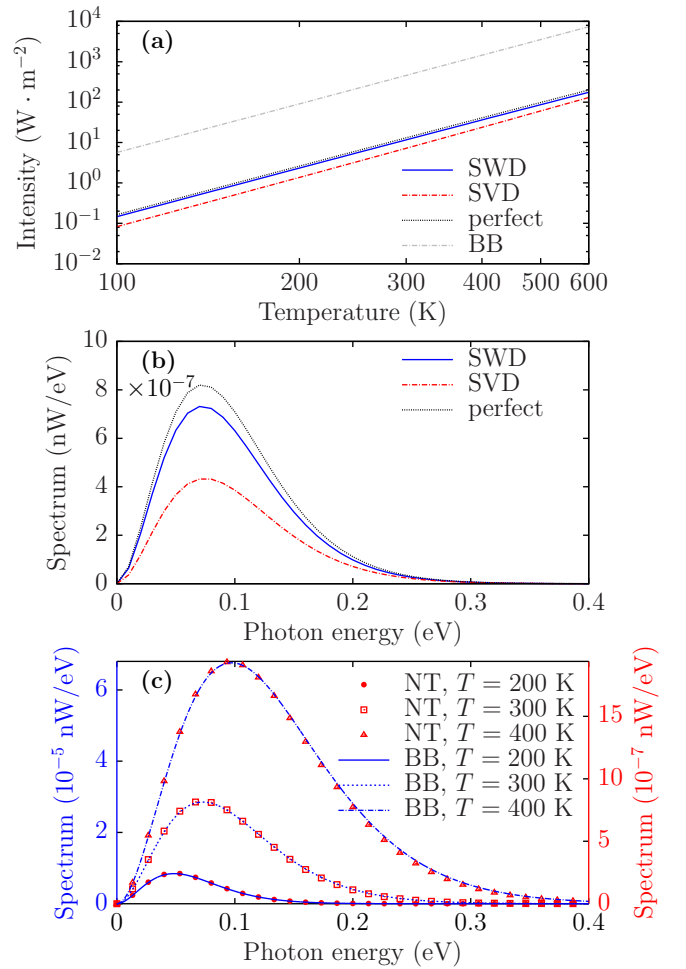


FIG. 4. Results of thermal radiation from the conducting channel of the two-terminal device using (7,7) CNT under zero bias. Temperatures of the two leads are the same. (a) Radiation intensity as a function of the temperature. (b) Spectrum of the radiation power with temperature $T = 300 \text{ K}$. (c) The radiation spectrum using the perfect CNT under different temperatures are compared with the spectrum of the black-body radiation with the same area as the CNT channel.

The longitudinal and transverse components of the conductivity are given by $\sigma_{\parallel} = \sigma_{zz}$, and $\sigma_{\perp} = \sigma_{xx} + \sigma_{yy}$, respectively. The spectrum of black-body radiation with the same area is $S_{\text{BB}}(\omega) = \frac{A\omega^3}{4\pi^2c^2} N_B(\omega)$. Comparing it with Eq. (6), we conclude that the strict condition for the shape of the radiation spectrum of a metallic material to fit with that of the black-body radiation is that the real part of the conductivity should be a constant in the energy range of thermal excitation. The black-body-like spectrum in Fig. 4(b) is determined to a large extent by the intrinsic nature of thermal equilibrium fluctuation, i.e., the factor $\omega^3 N_B(\omega)$ in Eq. (6), despite that the real parts of the conductivities for the channels using the perfect and defected CNTs in Fig. 5 are not strictly constant in the energy range of thermal excitation. For both the perfect and defected CNTs, the total conductivity is mainly contributed by the longitudinal component in the low-energy range, noting that the photon energy from thermal radiation is smaller than 0.5 eV, while the transverse component is only significant in the high-energy range. Thus, the thermal radiation is

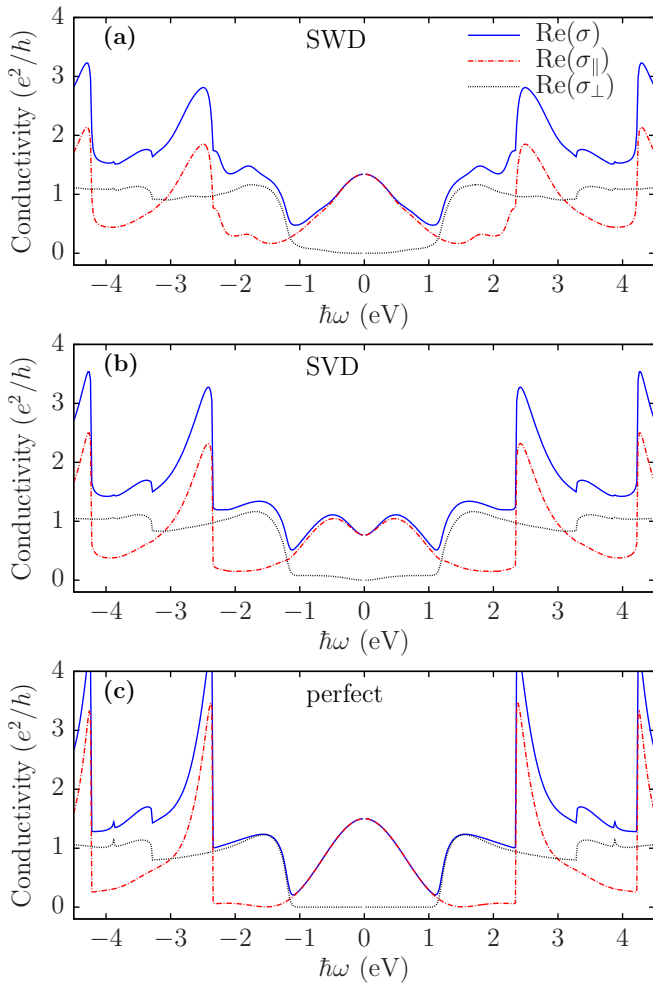


FIG. 5. Optical conductivity (real part) for the CNT channel of the device using the (7,7) CNTs at $T = 300$ K. σ , $\sigma_{||}$, and σ_{\perp} are the total conductivity, the longitudinal part and perpendicular part, respectively.

constrained in the circular direction of the CNTs. Finally, a quantitative analysis of the change of the magnitude of the spectrum due to the defects of CNTs in Fig. 4(b) can be attributed to the decrease of the optical conductivity by the defects shown in Fig. 5.

Finally, we make a few remarks on our results. First, the above numerical results are based on the ballistic transport regime. Phonon scattering can reduce the electron lifetime and broaden the electron density of states and the radiation spectrum. Applying a bias voltage across the CNTs can enhance the phonon scattering [51]. We explore the influence of the finite broadening effects due to electron-phonon interaction under a constant-relaxation time approximation (see the Appendix). We find that the broadening effects have very small influence on the radiation from CNTs with defects. For the perfect CNTs, they can enhance the radiation under the bias slightly lower than the onset bias and they can decrease the threshold bias. Second, we note that “metallic” zigzag or chiral carbon nanotubes with small energy gap due to strain or curvature effects [3,52] have very different optical properties in the low-energy range compared with gapless

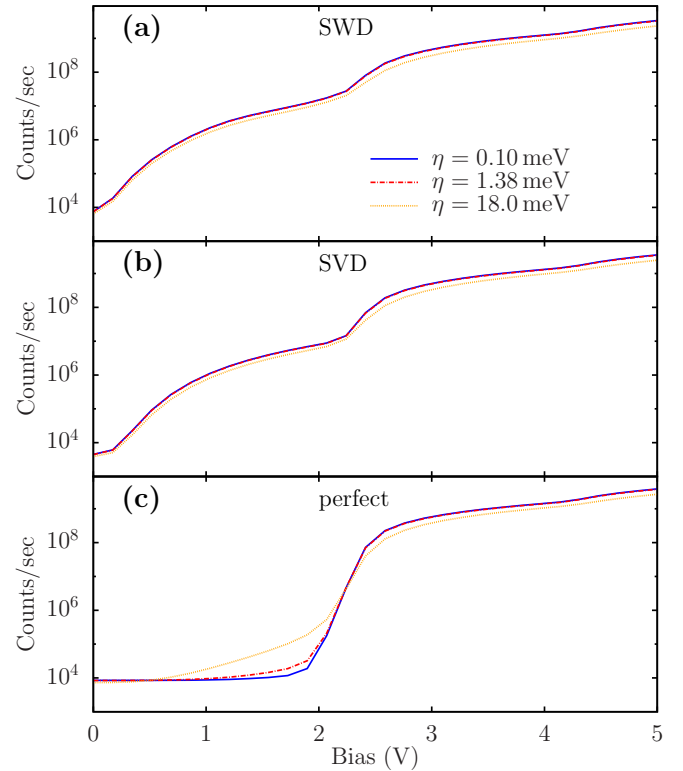


FIG. 6. Photon counts per second from the conducting channel of the two terminal device using (7,7) nanotubes at temperature $T = 300$ K with different broadening factors. The very small $\eta = 0.10$ meV is used for the ballistic transport.

armchair nanotubes. Optical transition is significant in the vicinity of the small energy gap, which has received intensive study theoretically and has been supported experimentally by observations of optical absorption in the far-infrared region [53–56]. The interplay between the localized states induced by the defects and the divergent joint density of states in the vicinity of the small band-gap edge in the nonarmchair “metallic” nanotubes are expected to play an important role in the electroluminescence, which would be an interesting topic for further study.

IV. SUMMARY

Using the NEGF method, we study EL and thermal radiation from metallic armchair SWCNTs with defects in the ballistic transport regime based on a tight-binding model. We find that both the SV defect and SW defect can enhance the EL, which increases exponentially in the low bias range, while for the perfect nanotube only thermal radiation contributes and the EL can be neglected. The enhancement of radiation due to the defects is not obvious in the high bias range, where strong radiation due to transitions between high-energy bands becomes dominant. The enhancement of the EL and the diameter of the CNT have a positive correlation in the presence of a SW defect, while for the CNT with a SV defect they have a negative correlation. Due to confinement of thermal excitation in the transverse direction, the intensity of the thermal radiation is independent of the nanotube diameter.

Defects can reduce the optical conductivity of the CNT, and they reduce the thermal radiation. This reducing effect is more significant for the CNT with a SV defect than that with a SW defect.

ACKNOWLEDGMENTS

We acknowledge the support by MOE tier 2 Grant No. R-144-000-411-112 and FRC Grant No. R-144-000-402-114.

APPENDIX: FINITE BROADENING EFFECTS

Due to electron-phonon interaction (EPI) in the CNTs, the corresponding density of states of the electrons and radiation spectrum would show some broadening effects compared to the ballistic transport case without EPI. The simplest way to consider the broadening effects is to use a constant relaxation-time approximation, which corresponds to use a finite η in

the GF $g^r(E) = [(E + i\eta)I - H_0 - \Sigma_{\text{leads}}^r]^{-1}$, i.e., by using $\eta = h/\tau$, with h the Planck constant and τ the relaxation time. The electrons are scattered mainly by acoustic phonons when the CNTs are under low bias, while the optical-phonon scattering becomes dominant in the high bias range. A typical relaxation time is $\tau \approx 3.0 \times 10^{-12}$ s for the first process and $\tau \approx 2.3 \times 10^{-13}$ s for the second process [51], corresponding to $\eta = 1.38$ meV, and $\eta = 18.0$ meV respectively.

It can be seen from Fig. 6 that very small decreasing of the radiation from the CNTs with defects are observed due to using a finite-broadening factor. For the perfect CNT, the broadening effects can lower the threshold bias, and the radiation can be enhanced a lot at the bias slightly lower than the threshold bias. Here we note that our simple way for the broadening effects by simply using a finite η can not account for the influence of the local EPI around the defects, which requires a more complex method combined with first-principle calculations and it is a challenging topic.

-
- [1] J.-C. Charlier, X. Blase, and S. Roche, *Rev. Mod. Phys.* **79**, 677 (2007).
- [2] M. Ouyang, J.-L. Huang, C. L. Cheung, and C. M. Lieber, *Science* **292**, 702 (2001).
- [3] J. Cao, Q. Wang, and H. Dai, *Phys. Rev. Lett.* **90**, 157601 (2003).
- [4] T. Ando, *J. Phys. Soc. Jpn.* **74**, 777 (2005).
- [5] J. A. Misewich, R. Martel, Ph. Avouris, J. C. Tsang, S. Heinze, and J. Tersoff, *Science* **300**, 783 (2003).
- [6] J. Chen, V. Perebeinos, M. Freitag, J. Tsang, Q. Fu, J. Liu, and Ph. Avouris, *Science* **310**, 1171 (2005).
- [7] J. Lefebvre and P. Finnie, *Phys. Rev. Lett.* **98**, 167406 (2007).
- [8] Ph. Avouris, M. Freitag, and V. Perebeinos, *Nat. Photon.* **2**, 341 (2008).
- [9] D. Mann, Y. K. Kato, A. Kinkhabwala, E. Pop, J. Cao, X. Wang, L. Zhang, Q. Wang, J. Guo, and H. Dai, *Nat. Nanotechnol.* **2**, 33 (2007).
- [10] L. Xie, H. Farhat, H. Son, J. Zhang, M. S. Dresselhaus, J. Kong, and Z. Liu, *Nano Lett.* **9**, 1747 (2009).
- [11] S. Essig, C. W. Marquardt, A. Vijayaraghavan, M. Ganzhorn, S. Dehm, F. Henrich, F. Ou, A. A. Green, C. Sciascia, F. Bonaccorso, K.-P. Bohnen, H. v. Löhneysen, M. M. Kappes, P. M. Ajayan, M. C. Hersam, A. C. Ferrari, and R. Krupke, *Nano Lett.* **10**, 1589 (2010).
- [12] M. Sveningsson, M. Jönsson, O. A. Nerushev, F. Rohmund, and E. E. B. Campbell, *Appl. Phys. Lett.* **81**, 1095 (2002).
- [13] P. Li, K. Jiang, M. Liu, Q. Li, S. Fan, and J. Sun, *Appl. Phys. Lett.* **82**, 1763 (2003).
- [14] J. Wei, H. Zhu, D. Wu, and B. Wei, *Appl. Phys. Lett.* **84**, 4869 (2004).
- [15] Y. V. Shtogun and L. M. Woods, *Carbon* **47**, 3252 (2009).
- [16] P. Partovi-Azar and A. Namiranian, *J. Phys.: Condens. Matter* **24**, 035301 (2011).
- [17] J. Wu, F. Hagelberg, T. C. Dinadayalane, D. Leszczynska, and J. Leszczynski, *J. Phys. Chem. C* **115**, 22232 (2011).
- [18] L. Chico, L. X. Benedict, S. G. Louie, and M. L. Cohen, *Phys. Rev. B* **54**, 2600 (1996).
- [19] H. J. Choi, J. Ihm, S. G. Louie, and M. L. Cohen, *Phys. Rev. Lett.* **84**, 2917 (2000).
- [20] N. Neophytou, S. Ahmed, and G. Klimeck, *Appl. Phys. Lett.* **90**, 182119 (2007).
- [21] F. Teichert, A. Zienert, J. Schuster, and M. Schreiber, *Comput. Mater. Sci.* **138**, 49 (2017).
- [22] G. Wei, *Appl. Phys. Lett.* **89**, 143111 (2006).
- [23] M. Buongiorno Nardelli, J.-L. Fattebert, D. Orlikowski, C. Roland, Q. Zhao, and J. Bernholc, *Carbon* **38**, 1703 (2000).
- [24] M. Sammalkorpi, A. Krasheninnikov, A. Kuronen, K. Nordlund, and K. Kaski, *Phys. Rev. B* **70**, 245416 (2004).
- [25] K. Sharma, K. K. Saxena, and M. Shukla, *Procedia Eng.* **38**, 3373 (2012).
- [26] H. Harutyunyan, T. Gokus, A. A. Green, M. C. Hersam, M. Allegrini, and A. Hartschuh, *Nano Lett.* **9**, 2010 (2009).
- [27] J. Mu, Y. Ma, H. Liu, T. Zhang, and S. Zhuo, *J. Chem. Phys.* **150**, 024701 (2019).
- [28] Y. Fan, B. R. Goldsmith, and P. G. Collins, *Nat. Mater.* **4**, 906 (2005).
- [29] A. H. Brozena, M. Kim, L. R. Powell, and Y. Wang, *Nat. Rev. Chem.* **3**, 375 (2019).
- [30] Y. Piao, B. Meany, L. R. Powell, N. Valley, H. Kwon, G. C. Schatz, and Y. Wang, *Nat. Chem.* **5**, 840 (2013).
- [31] X. He, N. F. Hartmann, X. Ma, Y. Kim, R. Ihly, J. L. Blackburn, W. Gao, J. Kono, Y. Yomogida, A. Hirano, T. Tanaka, H. Kataura, H. Htoon, and S. K. Doorn, *Nat. Photon.* **11**, 577 (2017).
- [32] A. Ishii, X. He, N. F. Hartmann, H. Machiya, H. Htoon, S. K. Doorn, and Y. K. Kato, *Nano Lett.* **18**, 3873 (2018).
- [33] R. Coratger, J.-P. Salvetat, A. Carladous, F. Ajustron, J. Beauvillain, J.-M. Bonard, and L. Forró, *Eur. Phys. J. Appl. Phys.* **15**, 177 (2001).
- [34] T. Uemura, S. Yamaguchi, M. Akai-Kasaya, A. Saito, M. Aono, and Y. Kuwahara, *Surf. Sci.* **600**, L15 (2006).
- [35] S. Katano, H. Fujita, and Y. Uehara, *Appl. Phys. Lett.* **112**, 011601 (2018).
- [36] M. Galperin and A. Nitzan, *Phys. Chem. Chem. Phys.* **14**, 9421 (2012).

- [37] J.-T. Lü, R. B. Christensen, and M. Brandbyge, *Phys. Rev. B* **88**, 045413 (2013).
- [38] K. Kaasbjerg and A. Nitzan, *Phys. Rev. Lett.* **114**, 126803 (2015).
- [39] K. Miwa, H. Imada, M. Imai-Imada, K. Kimura, M. Galperin, and Y. Kim, *Nano Lett.* **19**, 2803 (2019).
- [40] M. Parzefall and L. Novotny, *Rep. Prog. Phys.* **82**, 112401 (2019).
- [41] M. Ridley, L. Kantorovich, R. van Leeuwen, and R. Tuovinen, *Phys. Rev. B* **103**, 115439 (2021).
- [42] M. S. Purewal, B. H. Hong, A. Ravi, B. Chandra, J. Hone, and P. Kim, *Phys. Rev. Lett.* **98**, 186808 (2007).
- [43] K. Momma and F. Izumi, *J. Appl. Crystallogr.* **44**, 1272 (2011).
- [44] J.-S. Wang, J. Wang, and J. T. Lü, *Eur. Phys. J. B* **62**, 381 (2008).
- [45] J.-S. Wang, B. K. Agarwalla, H. Li, and J. Thingna, *Front. Phys.* **9**, 673 (2014).
- [46] Z.-Q. Zhang, J.-T. Lü, and J.-S. Wang, *Phys. Rev. B* **101**, 161406(R) (2020).
- [47] Y.-M. Zhang and J.-S. Wang, *J. Phys.: Condens. Matter* **33**, 055301 (2020).
- [48] M. B. Nardelli, *Phys. Rev. B* **60**, 7828 (1999).
- [49] J. W. Wilder, L. C. Venema, A. G. Rinzler, R. E. Smalley, and C. Dekker, *Nature (London)* **391**, 59 (1998).
- [50] M. Freitag, V. Perebeinos, J. Chen, A. Stein, J. C. Tsang, J. A. Misewich, R. Martel, and Ph. Avouris, *Nano Lett.* **4**, 1063 (2004).
- [51] J.-Y. Park, S. Rosenblatt, Y. Yaish, V. Sazonova, H. Üstüel, S. Braig, T. A. Arias, P. W. Brouwer, and P. L. McEuen, *Nano Lett.* **4**, 517 (2004).
- [52] S. Sreekala, X.-H. Peng, P. M. Ajayan, and S. K. Nayak, *Phys. Rev. B* **77**, 155434 (2008).
- [53] M. E. Itkis, S. Niyogi, M. E. Meng, M. A. Hamon, H. Hu, and R. C. Haddon, *Nano Lett.* **2**, 155 (2002).
- [54] S. Uryu and T. Ando, *Phys. Rev. B* **77**, 205407 (2008).
- [55] E. H. Hároz, J. G. Duque, X. Tu, M. Zheng, A. R. H. Walker, R. H. Hauge, S. K. Doorn, and J. Kono, *Nanoscale* **5**, 1411 (2013).
- [56] R. R. Hartmann, V. A. Saroka, and M. E. Portnoi, *J. Appl. Phys.* **125**, 151607 (2019).